Journal of Molecular Liquids 329 (2021) 115543

Contents lists available at ScienceDirect

Journal of Molecular Liquids

journal homepage: www.elsevier.com/locate/molliq

On the length of lecithin reverse wormlike micelles induced by inorganic salts: Binding site matters

Chia-Yi Lin, Shih-Huang Tung *

Institute of Polymer Science and Engineering and Advanced Research Center for Green Materials Science and Technology, National Taiwan University, Taipei 10617, Taiwan

ARTICLE INFO

Article history:
Received 5 December 2020
Received in revised form 26 January 2021
Accepted 29 January 2021
Available online 03 February 2021

Keywords:
Lecithin
Inorganic salt
Reverse wormlike micelle
Viscosity
Interaction

ABSTRACT

Previous studies have shown that the addition of inorganic salts to lecithin organosols induces long wormlike micelles that lead to organogels. The viscosity of the micellar solution greatly increases with the increasing concentration of the inorganic salt until gelation, but interestingly, it dramatically drops after the gel regime. Although the growth mechanism has been rationally proposed, the reason for the decrease in viscosity remains unclear. In this study, we investigated the rheological behaviors and the self-assembled structures of the lecithin wormlike micelles induced by LiCl, $CaCl_2$, and $LaCl_3$ in cyclohexane. We found that the decrease in viscosity accompanies a shortening in the length of the wormlike micelles. Meanwhile, the study on the interactions between lecithin and the inorganic salts by FTIR shows that the inorganic salts move from the saturated phosphate and choline region to the ester linkage region on lecithin as the viscosity drops. We suggest the movement of the excess inorganic salts alters the effective molecular geometry, which in turn breaks the long wormlike micelle into short ones, thus causing the viscosity to decrease. In other words, the binding sites of the inorganic salts in lecithin headgroups is a key factor that determines the self-assembled structures of lecithin reverse micelles.

1. Introduction

Amphiphiles, i.e., the molecules with hydrophilic segments and hydrophobic segments, can self-assemble into micelles both in aqueous and organic solutions when exceeding the critical micelle concentration [1]. In aqueous solutions, amphiphiles self-assemble into normal micelles with the hydrophilic headgroups facing outward to contact water and the hydrophobic tails burying in the cores [2–6]. The driving force for normal micelles is the hydrophobic interaction [7,8]. In low-polar organic solvents, amphiphiles organize reversely, so that the aggregates are called reverse or inverted micelles. The driving force for the reverse micelles is the interaction between the headgroups of amphiphiles, such as electrostatic interaction and hydrogen-bonding interaction [9–15]. In addition to the commonly-seen spherical micelles, wormlike micelles that are cylindrical in shape have drawn much attention due to their capability to entangle one another to significantly increases the solution viscosity, similar to the rheological behaviors of polymer chains. The shape of the self-assembled structures of amphiphiles can be simply explained by the theory of critical packing parameter (CPP) [16], which is defined by the ratio of the tail area to the headgroup area of amphiphiles.

Lecithin, a mixture of glycerophospholipids, is well-known to form reverse spherical or ellipsoidal micelles in a range of low-polar organic solvents. The main component in lecithin is illustrated in Fig. 1. The previous studies have shown that the lecithin reverse spherical micelles can be transformed into reverse wormlike micelles by incorporating additive molecules, such as water [11,17–20], bile salts [13,21–23], inorganic salts [12,14,24–26], and others with highly polar groups [27,28], into lecithin solution. The additives alone are generally insoluble in the low-polar organic solvents but become soluble in the presence of lecithin, indicating that there is an attractive force binding the additives and lecithin headgroup. Such a transformation is attributed to either the expansion of the lecithin headgroup area by insertion of the additives [13,21–23] or by straightening the lecithin tails that reduce the tail area due to the strong additive-lecithin attraction force [12,14,24], both of which alter the effective molecular geometry to a CPP that favors the formation of cylindrical micelles. The long, flexible cylindrical micelles thus increase the solution viscosity and even impart viscoelastic properties or further cause gelation. For the additives with large molecular size, such as bile salts [22], the viscosity increases monotonically with the concentration of the additives, that is, the viscosity keeps increasing until a critical additive concentration above which the solutions phase separate due to the insolubility of the additives in the solvents. In other words, the lecithin headgroup is unable to accommodate the bulky additives above the critical additive concentration. However, for small additives, such as water and inorganic salts [10–12,14,24,26,29], it is interesting that instead of monotonic increase, the viscosity reaches a maximum and then decreases until a phase separation occurs as the additive concentration increases. The viscosity

* Corresponding author.
E-mail address: shtung@ntu.edu.tw (S.-H. Tung).

https://doi.org/10.1016/j.molliq.2021.115543
0167-7322/

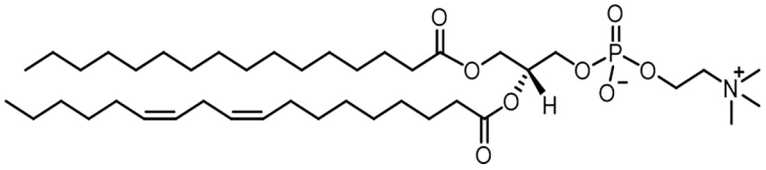

Fig. 1. Molecular structure of lecithin used in this study.

curves (in blue) shown in Fig. 2 are the examples caused by the inorganic salts.

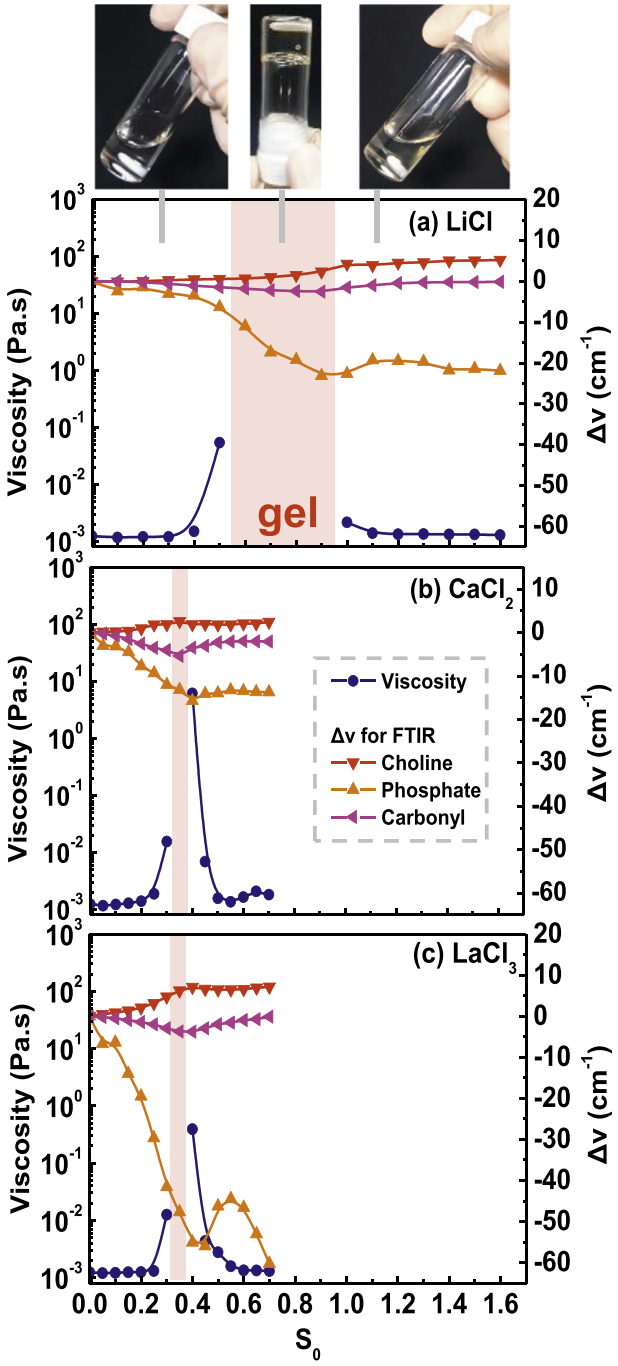

Fig. 2. Viscosity η_0 and FTIR band shifts $\Delta\nu$ of choline, phosphate, and carbonyl group on lecithin in cyclohexane at 25 °C as functions of S_0 for (a) LiCl, (b) $CaCl_2$, and (c) $LaCl_3$. Only the data of homogeneous samples are shown. The samples behave as gels in the shadow regions. Top images show the flow behaviors of the samples in different regimes.

The drop of the viscosity is intriguing. Shchipunov et al. proposed a mechanism to explain this phenomenon by investigating the rheological properties of the lecithin reverse wormlike micelles induced by water in *n*-decane [30]. They found that the dependence of the viscosity on the solute concentration follows the power law of linear micelles [31,32] in the regime where the viscosity increases and follows the power law of branched micelles [33–35] in the regime where the viscosity decreases. They thus concluded that the drop of viscosity is due to the transformation of linear cylindrical micelles to branched ones. They also utilized FTIR to investigate the hydrogen-bonding interaction between water and the functional groups on lecithin and suggested that the formation of the branch micelles is associated with the movement of the excess water molecules to the ester linkage region on lecithin when the primary binding site PO_4^- is saturated with water. In another report, though not focusing on the viscosity drop, Njauw et al. investigated the reverse micelles formed by lecithin mixed with bile salts/acids and found that for the bile salts/acids that insert into the ester linkage region on lecithin, their capability to enhance the viscosity is much lower than those that mainly locate in the phosphate and choline region [13].

Based on the above results, we believe that the location of the additives in the lecithin headgroup is key to determine the self-assembled structure and the corresponding rheological property of the lecithin reverse micelles. In this study, we explore the mechanisms for the decrease in the viscosity of the reverse micellar solutions as the additive exceeds a critical concentration. We adopt the systems of lecithin mixed with inorganic salts in cyclohexane. The inorganic salts we used include LiCl, $CaCl_2$, and $LaCl_3$, all of which are halide salts with the cations of different valences and can induce organogels at specific molar ratio of salt to lecithin. We investigated the rheological properties of the solutions and utilized the scattering and FTIR techniques to probe the self-assembled structures and the interactions between lecithin and the inorganic salts, respectively. Instead of the mechanism involving the transformation of linear micelles to branched micelles previously reported, we propose an alternative mechanism based on the change of the effective molecular geometry caused by the location of the inorganic salts to explain the growth and the shortening of the reverse wormlike micelles as the concentration of the inorganic salts increases.

2. Experimental section

2.1. Materials

The soybean lecithin (95% purity) was purchased from Avanti Polar Lipids, Inc. Inorganic salts, LiCl, $CaCl_2$, and $LaCl_3$, were in anhydrous form and the purities of all inorganic salts were higher than 99.9%. The purities of the anhydrous solvents, methanol and cyclohexane, were both 99.9%. All the salts and solvents were purchased from Sigma-Aldrich. All chemicals were used as received.

2.2. Sample preparation

Lecithin and inorganic salts were dissolved in anhydrous methanol to form 100 mM stock solutions, respectively. The stock solutions were then mixed with the required inorganic salt/lecithin molar ratio. After mixing, the samples were placed in a vacuum chamber to remove most methanol and then further dried in a vacuum oven at 55 °C for

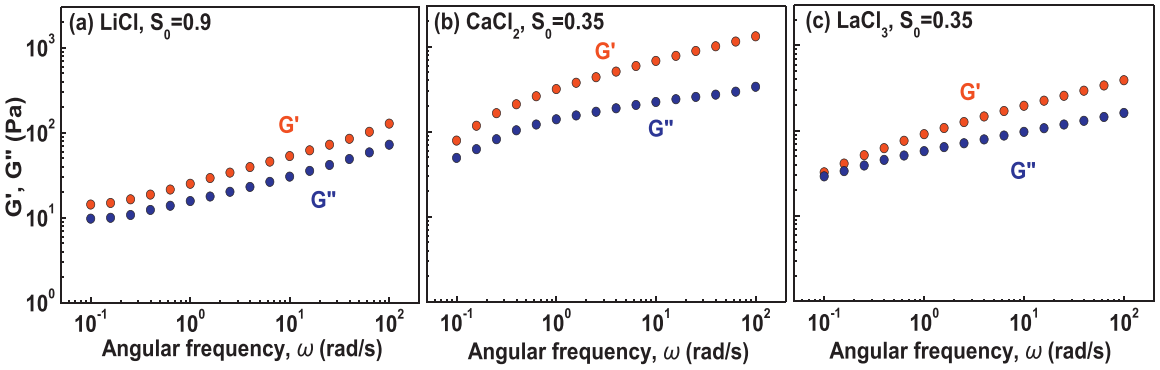

Fig. 3. Dynamic rheology of (a) LiCl, (b) $CaCl_2$, and (c) $LaCl_3$ samples in the gel regimes at 25 °C. The concentration of lecithin is 100 mM in cyclohexane.

72 h. Our previous study shows that after this processing, the molar ratio of lecithin to the residual water tightly bound to phosphate of lecithin is about 1:0.9 as determined by ^{1}H NMR [21]. The dried samples were added with cyclohexane at the desired concentrations and then stirred at 65 °C until the solutions were homogeneously mixed. All samples were equilibrated at room temperature for 3 days before experiments.

2.3. Rheology

Dynamic and steady-shear rheological experiments were performed on a Discovery HR-2 stress-controlled rheometer (TA instruments). The parallel-plate and cone-and-plate geometries were utilized with a solvent trap to minimize the evaporation of cyclohexane. All samples were studied at a lecithin concentration of 100 mM at 25 ± 0.1 °C. Dynamic rheology was studied in the linear viscoelastic regime determined by strain sweep tests. For steady-shear experiments, the data at each shear rate were collected after a sufficient time that allows the samples to reach steady state.

2.4. Fourier transform infrared spectrometry (FTIR)

FTIR transmission spectra were collected by a Perkin-Elmer Spectrum 100 FTIR spectrometer. Samples of 100 mM lecithin with different inorganic salt/lecithin molar ratios were loaded on the KBr liquid cell and measured in the wavenumber ranged from 450 to 4000 cm^{-1} at 25 °C. All spectra were collected under an accumulation of 16 scans at 1 cm^{-1} resolution. The signals of pure cyclohexane were subtracted from all the spectra.

2.5. X-ray scattering

Small/wide angle X-ray scattering (SAXS and WAXS) were made on BL23A in National Synchrotron Radiation Research Center (NSRRC), Taiwan [36]. For the SAXS experiments, the concentration of lecithin was diluted to 20 mM to remove the structure factor while that for the WAXS experiments was 100 mM. All the experiments were conducted at room temperature. The scattering of pure cyclohexane was taken as the background reference. The data were collected on a Pilatus 1 M-F detector and are shown as scattering intensity I versus wave vector $q = 4\pi\sin(\theta/2)/\lambda$, where θ is the scattering angle and λ is the wavelength.

2.6. SAXS modeling

The modeling of SAXS data was performed using the codes provided by NIST that are run in the Igor Pro software [37]. For dilute solutions of non-interacting scatterers, the SAXS intensity $I(q)$ is contributed from the form factor $P(q)$. In this study, we utilized the models of ellipsoid and cylinder with polydisperse length to fit the data, which are described below.

2.6.1. Ellipsoids

The form factor of ellipsoids with minor and major axes R_a and R_b is given by [38].

$$P(q) = (\Delta\rho)^2\left(\frac{4}{3}\pi R_a R_b^2\right)^2 \int_0^1 \left[3\frac{(\sin x - x\cos x)}{x^3}\right]^2 d\mu \quad (1)$$

where $x = q\sqrt{\mu^2 R_b^2 + R_a^2(1-\mu^2)}$ (2)

$\Delta\rho$ is the difference of the scattering length density between scatterer and solvent. μ is the cosine of the angle between the wave vector q and the symmetry axis of ellipsoids.

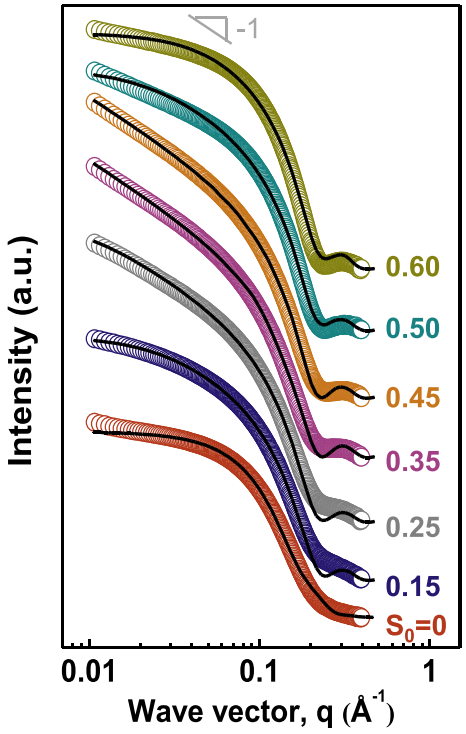

Fig. 4. SAXS data of $LaCl_3$/lecithin in cyclohexane at a lecithin concentration of 20 mM with varying S_0. Model fits are shown as the solid curves through the data.

Table 1
Fitting parameters from SAXS modeling.

S_0	R_a (Å)	R_b (Å)	R_c (Å)	L_0 (Å)	p_d
0	12.04 ± 0.06	28.55 ± 0.06			
0.15			16.45 ± 0.04	62.50 ± 1.80	0.79
0.25			16.42 ± 0.02	242.70 ± 1.93	0.53
0.35			16.44 ± 0.02	1325.57 ± 9.09	0.16
0.45			16.63 ± 0.02	1010.88 ± 6.46	0.59
0.50			16.68 ± 0.02	74.52 ± 0.38	0.78
0.60			16.93 ± 0.07	41.99 ± 1.01	0.63

2.6.2. Cylinders with polydisperse length

The form factor of a cylinder is given by [38].

$$P(q) = (\Delta\rho)^2\left(\pi R_c{}^2 L\right)^2 \int_0^{\pi/2} [F(q,\alpha)]^2 \sin\alpha\, d\alpha \tag{3}$$

$$F(q,\alpha) = \frac{J_1(qR_c\sin\alpha)}{(qR_c\sin\alpha)} \cdot \frac{\sin(qL\cos\alpha/2)}{(qL\cos\alpha/2)} \tag{4}$$

where L is the length of cylinder and R_c is the radius. α is the angle between the wave vector q and the cylinder axis. $J_1(x)$ is the first-order Bessel function of the first kind, given by

$$J_1(x) = \frac{\sin x - x\cos x}{x^2} \tag{5}$$

For cylinders with polydisperse length, the form factor is averaged over the length distribution as follows

$$P(q) = \int f(L)\cdot P(q,L)\, dL \tag{6}$$

where $P(q,L)$ is the form factor of a cylinder with length L (eq. 3). The polydispersity of length is described by the Schulz distribution $f(L)$, given by

$$f(L) = \left(\frac{z+1}{L_0}\right)^{z+1} \frac{L^z}{\Gamma(z+1)} \exp\left(-(z+1)\frac{L}{L_0}\right) \tag{7}$$

where L_0 is the average length, Γ is the Gamma function, and z is a parameter related to the distribution width. The polydispersity index p_d is defined by

$$p_d = \frac{1}{\sqrt{z+1}} \tag{8}$$

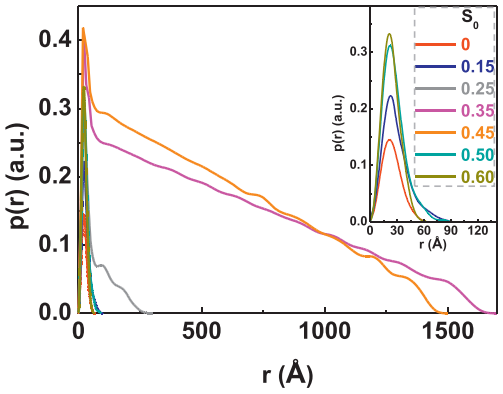

Fig. 5. Pair distance distribution functions $p(r)$ versus r obtained by IFT analysis of the SAXS data for the $LaCl_3$/lecithin mixtures. The inset is the enlarged plot of $p(r)$ at $r < 120$ Å.

2.7. Indirect Fourier transformation (IFT) of SAXS data

The SAXS data were also analyzed by the indirect Fourier transformation (IFT) method that requires no presumption of model. First, the incoherent background determined from the slope of the Porod plot (Iq^4 vs. q^4) at high q was subtracted from the scattering intensity. The subtracted scattering intensity $I(q)$ was then Fourier-transformed into the pair distance distribution function $p(r)$ in real space. For non-interacting scatterers, the relationship of $I(q)$ and $p(r)$ is given by [39]

$$I(q) = 4\pi\int_0^\infty p(r)\frac{\sin(qr)}{qr}dr \tag{9}$$

The IFT analysis was conducted by the commercial PCG software package. The data are shown as $p(r)$ versus r, which provides the size and the shape of the scatterers.

3. Results and discussion

3.1. Phase behaviors and rheological properties

Lecithin alone in low polar organic solvents self-assembles into ellipsoid micelles, which is nearly spherical micelles [12,21], and the viscosity is as low as that of cyclohexane below overlapping concentration [14]. The inorganic salts used in this study were LiCl, $CaCl_2$, and $LaCl_3$, which are unable to dissolve in cyclohexane but become soluble in the presence of lecithin. We first discuss the phase behaviors and rheological properties of the mixtures with varying inorganic salt/lecithin molar ratio S_0.

The dependence of the zero-shear viscosities (η_0) on S_0 for the inorganic salt/lecithin mixtures with lecithin concentration fixed at 100 mM are shown as the blue curves in Fig. 2. The steady shear viscosity data for the three salts are shown in Fig. S1, S2, and S3 of the supplementary data. In the shadow regions, no viscosity plateau is detected at low shear rate and the samples behave as gels. The data end at the S_0 below which the samples remain homogeneous and transparent, and

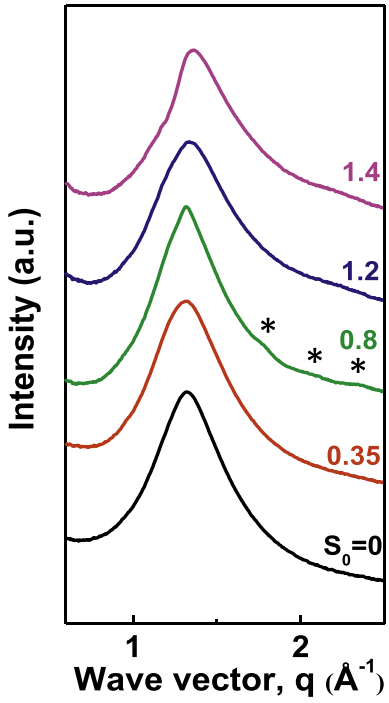

Fig. 6. WAXS data of LiCl/lecithin in cyclohexane at a lecithin concentration of 100 mM with varying S_0. The asterisks indicate the extra humps at $S_0 = 0.8$ in the gel regime.

the samples turn to be cloudy above this limit. Taking the LiCl salt in Fig. 2a as an example, at $S_0 < 0.4$, the viscosity is as low as that of pure lecithin in cyclohexane. At $S_0 = 0.5$, the viscosity increases markedly and the solution flows slowly in an inverted vial, indicating that the spherical micelles gradually transform into wormlike micelles that are sufficiently long to entangle one another. For S_0 between 0.6 and 0.9, the samples cannot flow in an inverted vial (see the photograph on the top of Fig. 2a). At this stage, the length of the wormlike micelles is long enough to cause a transient network with very long relaxation time such that no viscosity plateau can be measured by the rheometer in a practical time scale. In other words, the samples show a gel behavior. Interestingly, as S_0 keeps increasing, the viscosities drop dramatically and the samples restore the fluidity in an inverted vial. The S_0 where the organogels turn into organosols is denoted as S_{cr}, and for LiCl/lecithin mixtures, S_{cr} is 1.0. At $S_0 > S_{cr}$, the viscosity is as low as that before gelation, and the samples remain transparent until the phase separation occurs at $S_0 = 1.6$. The viscosity changes for $CaCl_2$/lecithin and $LaCl_3$/lecithin mixtures are similar to that of LiCl/lecithin but the S_0 for the gel formation and S_{cr} are lower, 0.35 and 0.40, respectively, for both $CaCl_2$ and $LaCl_3$, and the samples phase separate at $S_0 > 0.7$.

The viscoelasticity of the organogels were investigated by dynamic rheology. Fig. 3 shows the elastic modulus (G') and viscous modulus (G'') as functions of angular frequency (ω) for LiCl, $CaCl_2$, and $LaCl_3$ organogels at lecithin concentration 100 mM and $S_0 = 0.9$, 0.35, 0.35, respectively. The dynamic rheology of the LiCl organogels formed at other S_0s are shown in Fig. S4. For all the samples in Fig. 3, G' is higher than G'' in the entire angular frequency range, indicating a dominant elastic response of the organogels. However, unlike the true gel whose moduli are frequency-independent, the moduli decay with decreasing frequency and the gap between G' and G'' become narrower in these cases. Therefore, a long but finite relaxation time is expected for these samples. Such a rheological response is regarded as a gel-like behavior, not the typical criterion of true gels. The samples perform a gel-like behavior may be due to the formation of a transient network in the solutions by the entanglement of the exceedingly long and robust wormlike micelles that are unable to fully relax in practical time scales.

3.2. SAXS and WAXS

3.2.1. SAXS

The evolution of the self-assembled structures of the inorganic salt/lecithin mixtures in cyclohexane with S_0 was probed by SAXS at 25 °C. The concentration of lecithin was diluted to 20 mM to eliminate the structure factor because the main purpose of this study was to investigate the shape and size of the reverse micelles. The SAXS data for $LaCl_3$/lecithin mixtures with different S_0 are shown in Fig. 4, and those of the LiCl and $CaCl_2$ systems are shown in Fig. S5 and S7. The experimental data are presented as the circles and the solid curves through the data are the model fittings. The pure lecithin sample ($S_0 = 0$) was fitted by the ellipsoid model (eq. 1–2) while the others were fitted by the cylinder model with polydisperse length (eq. 3–8). The fitting parameters are listed in Table 1.

In Fig. 4, the SAXS profile of the pure lecithin ($S_0 = 0$) is relatively flat in the low q range, which can be modeled by a disk-like ellipsoid (oblate) with short axis $R_a = 12$ Å and long axis $R_b = 29$ Å. As S_0 increases from 0.15 to 0.35 between which the viscosity increases and the gelation occurs, the intensities of the profiles at low q gradually increases and the slope approaches −1, a scattering characteristic of cylinders. From the modeling, the length of the reverse cylindrical micelles longitudinally increases from 63 Å to 1326 Å. At $S_0 = 0.45$, the profile is similar to that at $S_0 = 0.35$, only a slight decrease in length to 1011 Å. For $S_0 > 0.45$ where the viscosity dramatically drops, the slopes at low q significantly decreases with the increasing S_0 and the length of the micelles decreases to 42 Å at $S_0 = 0.60$. The SAXS data can correlate with the change of viscosity well. At $S_0 < 0.25$, the micelles are either elliptic or short-cylindrical in shape, which can move freely, and thus the viscosity is low. Between $S_0 = 0.30$–0.40, the reverse micelles grow into long and flexible cylinders that entangle one another to greatly enhance viscosity and even lead to gelation. Near S_{cr} at 0.40, the length of the micelles reduces and the viscosity decreases accordingly as $S_0 > S_{cr}$.

In addition to the information of the length extracted from the low q range, the downturn around $q = 0.1$–0.2 Å^{-1} provides the information about the radius of the cylindrical micelles. In Table 1, the modeling shows that the radius R_c of the reverse wormlike micelles slightly increases from 16.45 Å at $S_0 = 0.15$ to 16.93 Å at $S_0 = 0.60$. Therefore, the addition of $LaCl_3$ affects not only the length but the radius of the reverse micelles. The scattering contrast for SAXS in the present system originates from the difference of the electron density between the lecithin headgroup coupled with inorganic salts and the tails swollen in cyclohexane. In other words, the radius obtained from the SAXS data is roughly the radius of the hydrophilic core of the cylinders, which is smaller than that obtained from the neutron scattering [12,14]. Since the inorganic salt are heavier than the organic lecithin headgroup, the location of the inorganic salts in the headgroup may play a role in the radius extracted from the SAXS modeling. The increasing radius implies that $LaCl_3$ gradually moves to the periphery of the hydrophilic core of the reverse micelles as S_0 increases, i.e., toward the ester linkages between the headgroups and the hydrophobic tails of lecithin, which we believe is responsible for the shortening of the chain length, as will be discussed in the mechanism section. The SAXS data of the LiCl/lecithin and $CaCl_2$/lecithin mixtures in Fig. S5 and S7 show similar trends of the length and radius changes with S_0 to that of $LaCl_3$ but the transition of the length may not exactly follow the viscosity change, which is possibly due to the different concentrations used in the rheological and scattering measurements.

In addition to the modeling, the SAXS data were analyzed in a different way by the IFT technique [39]. The pair distance distribution functions $p(r)$ calculated by the IFT method for the SAXS data of the $LaCl_3$/lecithin mixtures in Fig. 4 are shown in Fig. 5, and those of the LiCl and $CaCl_2$ systems are shown in Fig. S6 and S8, respectively. For the pure lecithin, $p(r)$ is almost symmetrical, indicative of nearly spherical micelles. The point where $p(r)$ meets the x-axis presents the largest dimension of the micelles, which is at $r = 60$ Å and is consistent with the double of R_b obtained from the SAXS modeling. As S_0 increases, the $p(r)$ shows an inflection and then an approximately linear decrease to zero, indicating that the micelles turn to be cylindrical. In these cases, the r value where the $p(r)$ drops to zero is the length of cylinder [39,40]. For the $LaCl_3$ system, the length of reverse wormlike micelles increases greatly from 82 Å at $S_0 = 0.15$ to 1657 Å at $S_0 = 0.35$, and then decreases sharply with increasing S_0 at $S_0 > 0.45$, in good agreement with the SAXS fitting parameters.

3.2.2. WAXS

The WAXS technique was used to investigate the molecular packing of lecithin in the reverse micelles with varying S_0 at a high lecithin concentration of 100 mM. Fig. 6 shows the WAXS data for the LiCl system. The pure lecithin ($S_0 = 0$) and the sample at $S_0 = 0.35$ show a broad peak at $q = 1.4$ Å^{-1}, which is the scattering halo from the loose packing of the lecithin molecules in the micelles. At $S_0 = 0.8$ where the gelation occurs, in addition to the 1.4 Å^{-1} peak, three extra humps at 1.7 Å^{-1}, 2.0 Å^{-1}, and 2.3 Å^{-1} appear, implying a regular molecular packing in the micelles of the LiCl-induced gel. Beyond the gel regime ($S_0 = 1.2$ and 1.4), the extra peaks disappear and the lecithin molecules are restored to the state of loose packing.The WAXS data reveal that the regular arrangements of lecithin occur only in the gel state where long cylindrical micelles are formed. At low S_0, the lecithin molecules arrange loosely in the nearly spherical or short cylindrical reverse micelles. At $S_0 > S_{cr}$, the length of the micelles is shortened and simultaneously the packing of the lecithin molecules turns back to the loose state. The WAXS data of the $CaCl_2$/lecithin and $LaCl_3$/lecithin organogels are shown in Fig. S9. The extra humps that appear in the LiCl gel cannot be clearly seen in the $CaCl_2$ and $LaCl_3$ gel. We speculate that the 1:1

binding between Li^+ and PO_4^- on the lecithin headgroup is favorable for molecular packing while 1:2 and 1:3 bindings for Ca^{2+} and La^{3+} may cause a crowding effect of the lecithin molecules around the high-valence cations and thus are unfavorable for a regular packing. This point will be elaborated in the mechanism section.

3.3. FTIR

The rheology data and scattering data have shown that inorganic salts play an important role in the structures of the lecithin reverse wormlike micelles. In this section, the FTIR techniques were utilized to investigate the interactions between the inorganic salts and the functional groups, including phosphate (PO_4^-), choline ($CN(CH_3)_3^+$), and carbonyl group (C = O), on lecithin to clarify the effects of the inorganic salts. The FTIR spectra of $CaCl_2$/lecithin mixtures are shown in Fig. 7 and those of the LiCl and $LaCl_3$ systems are shown in Fig. S10 and S11.

3.3.1. Phosphate

As the inorganic salts are mixed with the zwitterionic lecithin, they dissociate into metal cations and halide anions due to the strong electrostatic attraction between the metal cation ions and PO_4^- on lecithin, which is regarded as the primary force to induce the growth of wormlike micelles [14]. It has been reported that the asymmetrical vibrational mode of PO_4^- on lecithin dissolved in organic solvents is located at ~1260 cm^{-1}, and the band shifts to lower wavenumber (redshift) after inserting water [11] or inorganic salts in the lecithin headgroups [14]. Fig. 7a shows that the absorption band of PO_4^- on pure lecithin in cyclohexane is located at 1262 cm^{-1}, and it gradually redshifts to 1248 with increasing amount of $CaCl_2$ until $S_0 = 0.4$, indicating that more Ca^{2+} ions are bound to PO_4^- until the gel is formed. As $S_0 > 0.4$, the band stops redshifting, implying that the excess Ca^{2+} ions are no longer bound to PO_4^- above S_{cr} [11]. The band shift ($\Delta\nu$) of PO_4^- is compared to the viscosity curves with S_0 in Fig. 2b (orange curve) where we can see the viscosity increases with increasing strength of $Ca^{2+} - PO_4^-$ until the formation of organogels, and then drops dramatically when the binding between Ca^{2+} and PO_4^- is saturated. Similar trends are found for the LiCl or $LaCl_3$/lecithin mixtures in Fig. 2. The bands of PO_4^- above S_{cr} show some variations. This is possibly related to the fluctuation phenomenon near phase separation. Since the lecithin/inorganic salt systems above S_{cr} are about to phase separate, the salt concentration tends to locally fluctuate and an inhomogeneity in the solutions occurs. The local aggregation of salts may affect the interaction between the salts and PO_4^-. Because the interaction between $LaCl_3$ and lecithin headgroup is the strongest, the $LaCl_3$ system shows the most pronounced variation.

3.3.2. Choline

Fig. 7b shows the absorption band of the choline on lecithin in the $CaCl_2$/lecithin mixture with varying S_0. The choline band of pure lecithin in cyclohexane is at 969 cm^{-1}. As S_0 increases, opposite to PO_4^-, the band shifts to higher wavenumber (blueshift) until $S_0 = 0.35$ and then nearly fixes at 971 cm^{-1}. The shift of the choline band with S_0 is shown as the red curve in Fig. 2b. For pure lecithin in cyclohexane, the C–C single bond of O − C − C − N on lecithin tends to adopt a gauche conformation so that the positively charged choline associates with the negatively charged PO_4^- on the neighbor lecithin molecule [11], which is the driving force for the formation of the reverse micelles. In the mixture, choline should become bound to the negatively charged Cl^- dissociated from the salt as Ca^{2+} is strongly attracted to PO_4^- [14]. At $S_0 > S_{cr}$, the nearly constant choline band suggests that the amount of $CaCl_2$ in the ionic region of the lecithin headgroup is saturated near S_{cr}, in agreement with the shift of the PO_4^- band. Similar changes of the choline band can be seen in LiCl and $LaCl_3$ samples, as shown in Fig. 2.

3.3.3. Carbonyl

It has been reported that the stretching band of C=O on the ester linkage of pure lecithin dissolved in methanol is at 1744 cm^{-1} [13]. Fig. 7c shows the C=O band of pure lecithin in cyclohexane is at 1740 cm^{-1}, a redshift from that in methanol. Different from the isolated lecithin molecules dissolved in methanol, lecithin in cyclohexane self-assembles into nearly spherical micelles where the lecithin molecules aggregate. The polar C=O therefore forms strong dipole-dipole interaction with neighbor C=O to cause the redshift [14]. As S_0 increases, the band further shifts to lower wavenumber until $S_0 = 0.35$ in the gel regime although the redshift (1734 cm^{-1} at $S_0 = 0.35$) is not as

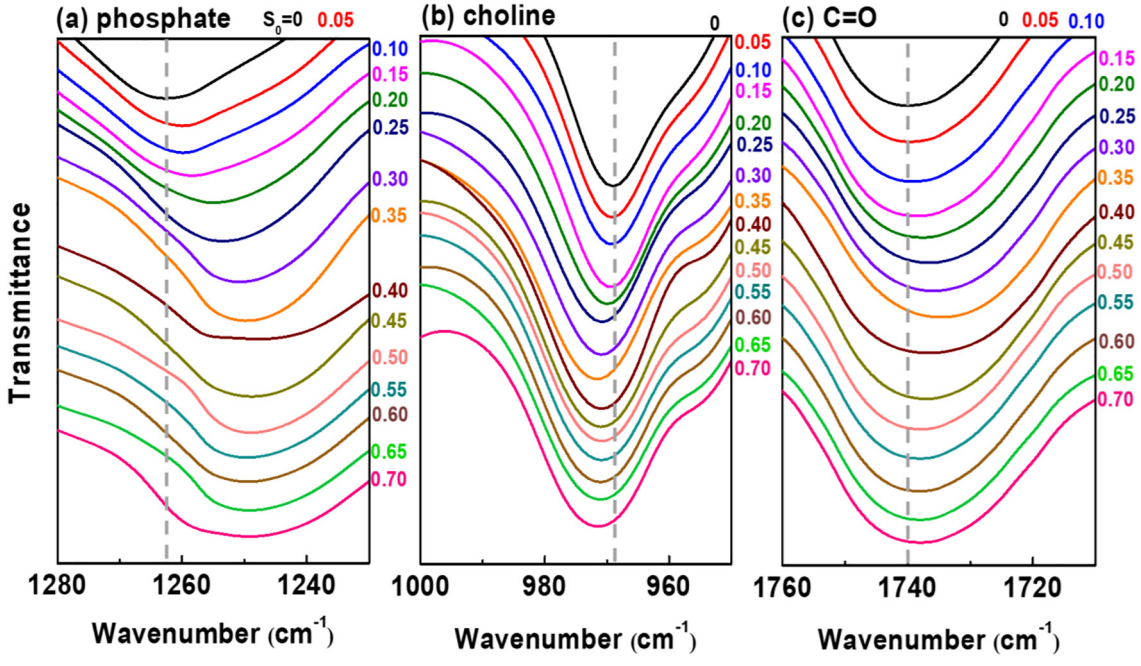

Fig. 7. FTIR absorption spectra of (a) phosphate, (b) choline, and (c) carbonyl group on lecithin for the $CaCl_2$/lecithin mixtures at varying S_0 in cyclohexane at 25 °C.

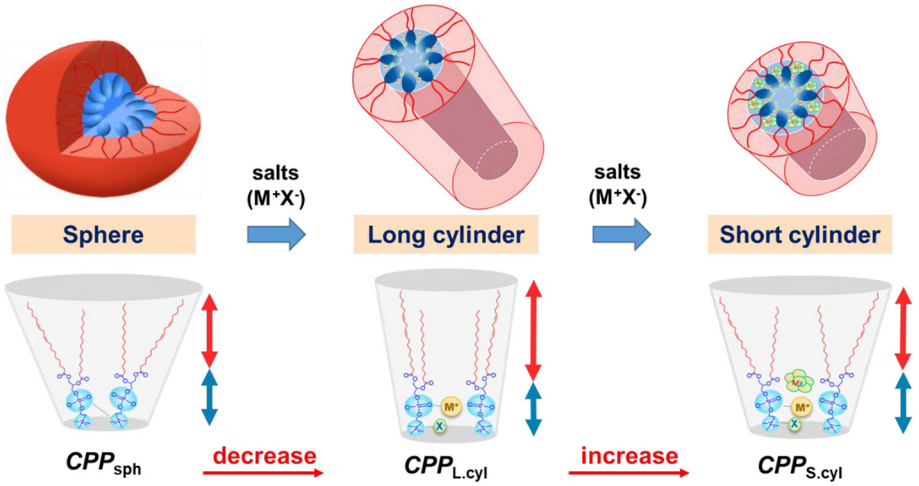

Fig. 8. Pure lecithin with swollen tails with large CPP forms nearly spherical micelles in cyclohexane. The binding of inorganic salts to the phosphate and choline on lecithin leads to more straightened tails and thus the CPP decreases to cause the long wormlike micelles. As more inorganic salts are added, the excess salts insert into the ester linkage on lecithin and disrupt the straightened tails, which in turn increases CPP to shorten the cylindrical micelles.

pronounced as that of PO_4^-. This is attributed to the strong binding between Ca^{2+} and PO_4^- that holds the lecithin molecules more tightly to enhance the dipole-dipole interaction between C=O groups [14]. At $S_0 > 0.4$ where the binding between Ca^{2+} and PO_4^- is saturated, interestingly, the C=O band moves to higher wavenumber (blueshift) with increasing S_0, back to 1738 cm^{-1} at $S_0 = 0.7$. This indicates that the intermolecular C=O dipole-dipole interaction is weakened in the presence of the excess $CaCl_2$.

The shifts of the C=O bands for the three salts are shown as the pink curves in Fig. 2. All the salts show similar shift curves with the minima in the gel regimes. This phenomenon can be explained as follows using $CaCl_2$ as an example. Above S_{cr}, since the binding between Ca^{2+} and PO_4^- is saturated, the excess $CaCl_2$ move from the PO_4^- and choline region to the polar ester linkage region where $CaCl_2$ is less dissociated due to the stronger Ca^{2+}– Cl^- electrostatic interaction over the Ca^{2+}-$O^{\delta-}$ ion-dipole interaction. Instead of binding to C=O, the less dissociated $CaCl_2$ mainly serves as a spacer that separates the C=O groups and weakens their dipole-dipole interaction, thus causing a blueshift in FTIR. The movement of $CaCl_2$ to the ester linkage region agrees with the increase in the cylinder radius as S_0 increases, as evidenced by the SAXS modeling (Table 1). Note that the molar ratio of $CaCl_2$ in the ester linkage region before phase separation is low, and thus $CaCl_2$ tends to weakly interact with the C=O rather than self-aggregate in a large scale. Some local aggregation may occur near the phase-separation critical point, but this doesn't affect the transparency of the samples.

3.4. Mechanisms

It has been well known that the self-assembled structure of amphiphiles in solutions is governed by the rule of CPP [16]. As shown in the schematic of Fig. 8, for pure lecithin in cyclohexane, the hydrophobic tails swell in the cyclohexane, leading to a larger tail area compared to headgroup area, which causes an effective molecular geometry that fit the curvature of nearly spherical reverse micelles. Below S_{cr}, the inorganic salts dissociate and the cation and anion bind to PO_4^- and choline on lecithin headgroup, respectively. The binding of the inorganic salts holds lecithin more tightly through the strong electrostatic interactions, as revealed by the redshifts of C=O absorption bands. The lecithin molecules are thus more straightened and more densely packed, as evidenced by the WAXS for the LiCl gels, which reduces the tail area and transforms the nearly spherical micelles into cylindrical ones. The cylindrical micelles are long and robust enough to form a transient network with a long relaxation time so that the viscosity is greatly increased and the solutions even behave like a gel. In the cartoons of Fig. 8, the blue cores of the micelles are approximately composed of the hydrophilic lecithin headgroups and the inorganic salts. The radii of the cores can be determined by the SAXS modeling due to the higher electron density compared to the hydrophobic tails swollen in cyclohexane.

Once the PO_4^- and choline are saturatedly bonded with the salts, the excess salts move to the ester linkages, which is supported by the increasing radius estimated from the SAXS modeling. The excess salts only weakly interact with the partially negatively charged $O^{\delta-}$ on the ester linkages and thus they work as the spacer that separates the tails, as evidenced by the blueshifts of the C=O band above S_{cr}, which in turn disrupts the regular packing of the tails and the tail area expands accordingly. Such an effective molecular geometry that fits higher curvature structure causes the formation of more hemispherical endcaps, and thus the long cylindrical micelles break into short ones. This explains why the viscosity sharply decreases. In addition to the inorganic salts, it has been reported that the insertion of bile salts into PO_4^- and choline region causes an increase in the viscosity of the lecithin reverse micellar solutions while the insertion of bile acids into the ester linkages does not have the same effect [13]. All the results manifest the crucial role of the binding location of the additives in the structure and rheological behaviors of lecithin reverse micelles.

Lastly, the effects of the salt valence are discussed. The experimental data reveal that S_{cr} is valence-dependent and is approximately the salt/lecithin molar ratio where the binding between salts and PO_4^- on lecithin is saturated. S_{cr} for LiCl is 1.0, which is rational because to maintain electrically neutral, one monovalent cation Li^+ must bind to one monovalent anion PO_4^-. As expected, S_{cr} for $CaCl_2$ is 0.4, indicating one Ca^{2+} approximately bind to two PO_4^- groups. However, for the trivalent $LaCl_3$, S_{cr} is still 0.4, not lower. We speculate that because the lecithin headgroup is much bulkier than the cations, three PO_4^- groups are too crowded to bind to one La^{3+} together and thus it is possible that only two PO_4^- groups and one Cl^- make the binding with La^{3+}, which explains why S_{cr} is the same as the divalent $CaCl_2$. The crowding effect found in the multivalent salts may be responsible for the less regular packing of lecithin molecules in gels induced by $CaCl_2$ and $LaCl_3$ as shown in the WAXS measurements (Fig. S9).

4. Conclusions

In this work, we shed light on the mechanisms for the structural evolution of lecithin reverse wormlike micelles. We systematically study

the lecithin reverse worms induced by inorganic salts, and correlate the rheological properties with the self-assembled structures and the interactions between lecithin and salts. Our main finding is that as the inorganic salts primarily bind to the phosphate and choline on lecithin headgroup, the lecithin tails are straightened and the lecithin reverse micelles tend to grow longitudinally, which causes the viscosity to increase. Once the phosphate and choline are saturated and the excess inorganic salts move to the ester linkages, the salts trigger a fluctuation of the tails, which is unfavorable for the formation of long micelles and thus the viscosity decreases. The results highlight the importance of the location of the inorganic salts in the self-assembly of lecithin reverse micelles. We believe that this argument can also be applied to the more widely studied lecithin/water/organic solvent systems. Moreover, although we focus on the reverse system, the findings in this work may be significant as well for the aqueous systems where the interaction between the inorganic salts and lipid bilayers is critical in physiological functions.

Declaration of Competing Interest

There are no conflicts of interest to declare.

Acknowledgements

This work was financially supported in part by the "Advanced Research Center of Green Materials Science and Technology" from the Featured Area Research Center Program within the framework of the Higher Education Sprout Project, and in part by S.-H.T's research fundings, granted by the Ministry of Education, Taiwan (109L9006 and 109L893402) and the Ministry of Science and Technology, Taiwan (MOST 106-2628-E-002-006-MY3, 109-2634-F-002-042, and 108-2923-E-002-001-MY3). The authors thank National Synchrotron Radiation Research Center, Taiwan, for facilitating the X-ray scattering experiments.

Appendix A. Supplementary data

Supplementary data to this article can be found online at https://doi.org/10.1016/j.molliq.2021.115543.

References

[1] E. Ruckenstein, R. Nagarajan, Critical micelle concentration. Transition point for micellar size distribution, J. Phys. Chem. 79 (1975) 2622.
[2] Y. Okahata, T. Kunitake, Self-assembling behavior of single-chain amphiphiles with the biphenyl moiety in dilute aqueous solution, Ber. Bunsenges. Phys. Chem. 84 (1980) 550.
[3] A.P. Nowak, V. Breedveld, L. Pakstis, B. Ozbas, D.J. Pine, D. Pochan, T.J. Deming, Rapidly recovering hydrogel scaffolds from self-assembling diblock copolypeptide amphiphiles, Nature 417 (2002) 424.
[4] J.D. Hartgerink, E. Beniash, S.I. Stupp, Peptide-amphiphile nanofibers: a versatile scaffold for the preparation of self-assembling materials, Proc. Natl. Acad. Sci. 99 (2002) 5133.
[5] J.S. Martinez, G.P. Zhang, P.D. Holt, H.T. Jung, C.J. Carrano, M.G. Haygood, A. Butler, Self-assembling amphiphilic siderophores from marine bacteria, Science 287 (2000) 1245.
[6] Y.X. Huang, R.C. Tan, Y.L. Li, Y.Q. Yang, L. Yu, Q.C. He, Effect of salts on the formation of C(8)-lecithin micelles in aqueous solution, J. Colloid Interface Sci. 236 (2001) 28.
[7] S. Krimm, The hydrophobic effect: formation of micelles and biological membranes, J. Polym. Sci. 18 (1980) 687.
[8] M.V. Poteshnova, N.M. Zadymova, Normal micelles and oil-in-water microemulsions in a water-toluene-tween 80 ternary system, Colloid J. 68 (2006) 201.
[9] P. Schurtenberger, R. Scartazzini, L.J. Magid, M.E. Leser, P.L. Luisi, Structural and dynamic properties of polymer-like reverse micelles, j, Phys. Chem. 94 (1990) 3695.
[10] Y.A. Shchipunov, E.V. Shumilina, Lecithin bridging by hydrogen bonds in the organogel, Mater. Sci. Eng. C 3 (1995) 43.
[11] E.V. Shumilina, Y.L. Khromova, Y.A. Shchipunov, A study of the structure of lecithin organic gels by IR spectroscopy with Fourier-transform, Russ. J. Phys. Chem. 74 (2000) 1210.
[12] H.-Y. Lee, K.K. Diehn, S.W. Ko, S.-H. Tung, S.R. Raghavan, Can simple salts influence self-assembly in oil? Multivalent Cations as efficient Gelators of lecithin Organosols, Langmuir 26 (2010) 13831.
[13] C.-W. Njauw, C.-Y. Cheng, V.A. Ivanov, A.R. Khokhlov, S.-H. Tung, Molecular interactions between lecithin and bile salts/acids in oils and their effects on reverse micellization, Langmuir 29 (2013) 3879.
[14] S.-T. Lin, C.-S. Lin, Y.-Y. Chang, A.E. Whitten, A. Sokolova, C.-M. Wu, V.A. Ivanov, A.R. Khokhlov, S.-H. Tung, Effects of alkali cations and halide anions on the self-assembly of phosphatidylcholine in oils, Langmuir 32 (2016) 12166.
[15] K. Hashizaki, T. Chiba, H. Taguchi, Y. Saito, Highly viscoelastic reverse worm-like micelles formed in a lecithin/urea/oil system, Colloid Polym. Sci. 287 (2009) 927.
[16] J. Israelachvili, Intermolecular and Surface Forces, 3rd edition Academic Press, 2011.
[17] R. Scartazzini, P.L. Luisi, Organogels from lecithins, J. Phys. Chem. 92 (1988) 829.
[18] D.M. Willard, R.E. Riter, N.E. Levinger, Dynamics of polar solvation in lecithin/water/cyclohexane reverse micelles, J. Am. Chem. Soc. 120 (1998) 4151.
[19] Y.A. Shchipunov, Lecithin organogel: a micellar system with unique properties, Colloids Surf. A Physicochem. Eng. Asp. 183-185 (2001) 541.
[20] S.-H. Tung, Y.-E. Huang, S.R. Raghavan, Contrasting effects of temperature on the rheology of normal and reverse wormlike micelles, Langmuir 23 (2007) 372.
[21] S.-H. Tung, Y.-E. Huang, S.R. Raghavan, A new reverse wormlike micellar system: mixtures of bile salt and lecithin in organic liquids, J. Am. Chem. Soc. 128 (2006) 5751.
[22] L.K. Shrestha, T. Sato, M. Dulle, O. Glatter, K. Aramaki, Effect of lipophilic tail architecture and solvent engineering on the structure of trehalose-based nonionic surfactant reverse micelles, J. Phys. Chem. B 114 (2010) 12008.
[23] L. Shrestha, R. Shrestha, M. Abe, K. Ariga, Reverse micelle microstructural transformations induced by oil and water, Soft Matter 7 (2011) 10017.
[24] H.-M. Chang, C.-Y. Lin, S.-H. Tung, Correlation between temperature-dependent rheology and electrostatic interactions in reverse wormlike micelles induced by inorganic salts, Soft Matter 16 (2020) 3505.
[25] H.-J. Lee, H.-J. Kim, D.-G. Park, K.S. Jin, J.W. Chang, H.-Y. Lee, Mechanism for transition of reverse cylindrical micelles to spherical micelles induced by diverse alcohols, Langmuir 36 (2020) 8174.
[26] C.-R. Lee, Y.-K. Lee, E.-J. Oh, K.S. Jin, H.-Y. Lee, Effect of aliphatic solvents on the reverse self-assembly of lecithin and calcium chloride mixtures, J. Mol. Liq. 316 (2020) 113790.
[27] K. Hashizaki, M. Imai, S. Yako, H. Tsusaka, Y. Sakanishi, Y. Saito, M. Fujii, Highly viscoelastic reverse wormlike micellar systems from a mixture of lecithin, polyglycerol fatty acid monoesters, and an oil, J. Oleo Sci. 66 (2017) 997.
[28] M. Imai, K. Hashizaki, H. Taguchi, Y. Saito, S. Motohashi, A new reverse worm-like micellar system from a lecithin, multivalent carboxylic acid and oil mixture, J. Colloid Interface Sci. 403 (2013) 77.
[29] Y.A. Shchipunov, E.V. Shumilina, Lecithin organogels: role of polar solvent and nature of intermolecular interactions, Colloid J. 58 (1996) 117.
[30] Y.A. Shchipunov, H. Hoffmann, Growth, branching, and local ordering of lecithin polymer-like micelles, Langmuir 14 (1998) 6350.
[31] M.E. Cates, Reptation of living polymers: dynamics of entangled polymers in the presence of reversible chain-scission reactions, Macromolecules 20 (1987) 2289.
[32] M.E. Cates, Nonlinear viscoelasticity of wormlike micelles (and other reversibly breakable polymers), J. Phys. Chem. 94 (1990) 371.
[33] F. Lequeux, Reptation of connected wormlike micelles, Europhys. Lett. 19 (1992) 675.
[34] J. Appell, G. Porte, A. Khatory, F. Kern, S.J. Candau, Static and dynamic properties of a network of wormlike surfactant micelles (cetylpyridinium chlorate in sodium chlorate brine), J. Phys. II France 2 (1992) 1045.
[35] A. Khatory, F. Kern, F. Lequeux, J. Appell, G. Porte, N. Morie, A. Ott, W. Urbach, Entangled versus multiconnected network of wormlike micelles, Langmuir 9 (1993) 933.
[36] U.-S. Jeng, C.H. Su, C.-J. Su, K.-F. Liao, W.-T. Chuang, Y.-H. Lai, J.-W. Chang, Y.-J. Chen, Y.-S. Huang, M.-T. Lee, K.-L. Yu, J.-M. Lin, D.-G. Liu, C.-F. Chang, C.-Y. Liu, C.-H. Chang, K.S. Liang, A small/wide-angle X-ray scattering instrument for structural characterization of air–liquid interfaces, thin films and bulk specimens, J. Appl. Crystallogr. 43 (2010) 110.
[37] S.R. Kline, Reduction and analysis of SANS and USANS data using IGOR pro, J. Appl. Crystallogr. 39 (2006) 895.
[38] J.S. Pedersen, Analysis of small-angle scattering data from colloids and polymer solutions: modeling and least-squares fitting, Adv. Colloid Interf. Sci. 70 (1997) 171.
[39] O. Glatter, A new method for the evaluation of small-angle scattering data, J. Appl. Crystallogr. 10 (1977) 415.
[40] T.S. Davies, A.M. Ketner, S.R. Raghavan, Self-assembly of surfactant vesicles that transform into viscoelastic wormlike micelles upon heating, J. Am. Chem. Soc. 128 (2006) 6669.